Mechanics of Time-Dependent Materials (2022) 27:185–205
https://doi.org/10.1007/s11043-021-09530-z

Functionalized graphene–epoxy nanocomposites: experimental investigation of viscoelastic and viscoplastic behaviors

Ozgen U. Colak[1] · Besim Birkan[1] · Okan Bakbak[1] · Alperen Acar[1] · Deniz Uzunsoy[2]

Received: 12 August 2021 / Accepted: 2 December 2021 / Published online: 22 January 2022
© The Author(s), under exclusive licence to Springer Nature B.V. 2021

Abstract
In this work, graphene–epoxy nanocomposites are produced for two different graphene fractions (0.1 and 0.5 wt%). Three-roll milling is used as the main strategy to achieve a homogeneous dispersion and prevent agglomeration. To improve the interfacial bonding between graphene nanoflakes (GNF) and epoxy matrix, GNFs are functionalized using Triton X-100 as a surfactant. The effectiveness of this functionalization is investigated using Raman spectroscopy and Fourier transform infrared spectroscopy (FT-IR). These spectroscopy results show that the Triton X-100 molecules are successfully adsorbed on the surface of GNFs. To investigate the total viscoelastic–viscoplastic behavior of the nanocomposites, compression tests at three different quasistatic strain rates (1.E-1, 1.E-2, 1.E-3 /s), creep tests at two different stress levels and relaxation tests at two different strain levels are performed. The total time-dependent mechanical behavior of the produced nanocomposites is therefore characterized comprehensively. Elasticity-modulus values obtained from compression tests increased up to 29% and yield stress increased up to 18%. In creep tests, it is observed that the creep strain decreased 32% and 65% at 50 and 100 MPa stress levels, respectively, at 0.1 wt% functionalized graphene flakes (f-GNF)–epoxy nanocomposite. At the same time, with the addition of 0.1 wt% f-GNF to epoxy, during relaxation tests, the stress drop decreased up to 47% compared to pure epoxy at a 3.16% constant strain level. Both creep and relaxation resistance improved when compared to pure epoxy. This total improvement in the mechanical behaviors is explained with the effective dispersion of the GNFs and also a strong interface between the GNFs and the epoxy matrix.

Keywords Polymer–matrix composites (PMCs) · Creep · Stress relaxation · Mechanical testing · Graphene–epoxy

1 Introduction

Graphene, which consists of a two-dimensional (2D) sheet of covalently bonded carbon atoms, has attracted a great deal of attention due to its excellent physical, thermal, and electrical properties. With a theoretically calculated and experimentally measured elasticity modulus of 1 TPa, graphene is one of the strongest materials ever tested. The thermal conductivity of a single graphene layer is measured to be in the range of ∼3080–5150 W/m K

Extended author information available on the last page of the article

(Balandin et al. 2008). These properties of graphene make it a great filler material for epoxy-based composites. In addition, graphene costs are lower than many other filler materials (carbon nanotubes, etc.) because of its ease of manufacturing. Graphene–epoxy nanocomposites are starting to find application areas in many different industries, from aerospace to automotive.

The main challenge of the manufacturing process of nanocomposites is dispersing graphene homogeneously inside the matrix material. Optimum enhancement in the mechanical properties can be achieved only when the filler material (GNFs) is uniformly dispersed. To provide uniform dispersion, several techniques such as ultrasonic methods, high- and low-shear mixing, and functionalization of graphene sheets have been reported in the literature (Martin-Gallego et al. 2018). Two of the most used methods are sonication and three-roll milling (3RM). The sonication method uses pulsed ultrasound to exfoliate agglomerations and disperse GNFs in the matrix material. The 3RM method works on the principle of creating shear stress on the material by using three rollers rotating in opposite directions and at different speeds. This principle enables GNFs to disperse in highly viscous materials, which in this study is an epoxy resin. Unlike the sonication method, exfoliation of GNF agglomerations can be achieved with the 3RM method utilizing its adjustable gap distance up to 5 μm (Chandrasekaran et al. 2013). Prolongo et al. compared three-roll milling and high-shear mixing and recommended the three-roll milling method for enhanced mechanical properties (Prolongo et al. 2013). In the work by Moriche et al. (Moriche et al. 2015), it is shown that when only sonication is applied, GNFs are wrinkled into the nanocomposites and these wrinkles caused higher residual stresses when the resin is cured. When 3RM is involved, sheets are flattened by the applied shear forces, which leads to reducing strains in the nanoplatelets and decreasing residual stresses (Moriche et al. 2015). A detailed literature review showed that using the 3RM method for dispersing GNFs in the matrix material for producing nanocomposites promises great improvement in the mechanical properties and electrical–thermal conductivity (Chandrasekaran et al. 2014; Hashim and Jumahat 2018; Imran and Shivakumar 2018).

Another problem to overcome with nanocomposites using graphene as a filler material is the interface interaction between the two phases of the composite. The reason for the agglomeration of graphene platelets is the Van der Waals forces between the graphene sheets (McAllister et al. 2007). Tailoring of the interface between graphene and the matrix is therefore critical for a homogeneous dispersion and a lower rate of agglomeration. To overcome this negative effect, two methods are mainly used in the literature. The first of these is covalent bonding by the addition of functional oxygen groups to graphene. The second method is the noncovalent attachment of molecules to graphene-platelet surfaces. The most common examples of noncovalent functionalization are polymer wrapping, surfactant absorption, p–p interactions and hydrogen bonding (Dai et al. 2016; Georgakilas et al. 2016). Li et al. used poly(sodium 4-styrene sulfonate) (PSS) to noncovalently functionalize graphene and introduce the graphene into an epoxy resin to form nanocomposites and reported improved tensile strength and modulus (Li et al. 2015). Zhang et al. studied both noncovalent and covalent methods and reported that using Triton X-100 surfactant for the treatment of graphene led to nanocomposites with improved properties (Zhang et al. 2016). In summary, the literature review reveals that the noncovalent method (using Triton X-100 as a surfactant) for functionalizing graphene is promising to obtain enhanced mechanical properties (Anwer et al. 2019; Dai et al. 2016; Wan et al. 2013).

Because of the increasing interest and widened applications of nanocomposites, all viscoelastic and viscoplastic behaviors such as rate dependency, creep, relaxation, recovery, and the mechanical properties need to be studied. Shadlou et al. (Shadlou et al. 2014) studied the strain-rate behavior of GNF-reinforced epoxy nanocomposites. The results showed

that yield strength and Young's modulus increased at higher strain rates. Chandrasekaran et al. prepared graphene–epoxy specimens using the 3RM method and observed a 17% increase in the storage modulus (Chandrasekaran et al. 2013). In the literature, it is shown that the addition of GNFs to the epoxy using the 3RM method increased the mechanical properties of the prepared nanocomposites (Ahmadi-Moghadam and Taheri 2014; Chandrasekaran et al. 2014; Wang et al. 2015a, 2015b).

In this work, specimens were produced with a different method when compared to the literature, which consists of functionalization of the graphene sheets with Triton X-100 and then using the 3RM method to uniformly disperse GNFs in the epoxy matrix. Specimens were produced with the three-roll milling method using different cycles to determine the best number of cycles to use when producing nanocomposites to prevent agglomeration. Differences in elasticity modulus and yield strength have been experimentally investigated and reported for the different number of cycles (5, 6, 7, 8 cycles). Raman spectroscopy is conducted on pristine and functional graphene. FT-IR was performed to investigate the molecular orientation and types of bonds and molecules of GNF and graphene functionalized with Triton X-100 to produce functionalized graphene (f-GNF). For mechanical characterization, three different types of tests were conducted. These were compression tests at different strain rates (1.E-1, 1.E-2 and 1.E-3 /s), creep and relaxation tests at different constant stress (50 and 100 MPa) and constant strain levels (3.16 and 7.15%). Creep and relaxation tests conducted for determining the viscoelastic properties of the produced nanocomposites were made for a duration of 2 h, which differs from the similar studies in the literature. The improvements are observed in the elasticity modulus, yield strength and creep and relaxation resistance in the nanocomposite. This improvement in the mechanical behavior is increased with increasing f-GNF concentration, which is also taken as proof of the effective dispersion and the strong interfacial bond that is achieved.

2 Materials and methods

2.1 Materials

The epoxy system used as the matrix material in this study is Araldite LY 564 with hardener Aradure 2954. This epoxy system supplied from Hunstman CO has a high glass transition temperature (Tg) and elasticity modulus. The Tg value of the epoxy system is 80–87 °C if determined by thermomechanical analysis (TMA) and 99–105 °C if determined by differential scanning calorimetry (DSC). In Malysheva's work, the pure epoxy's Tg value is determined as 120.03 °C (Malysheva et al. 2014). Araldite LY 564's elasticity modulus values are 1920–2050 MPa according to Bakbak et al. (Bakbak et al. 2021). It is used in a wide range of applications from ballistic-armor, aerospace applications to composite materials used for structural designs. Graphene was used as the reinforcement material in this study. There are many different synthesis methods of graphene. Here, graphene was synthesized by the electric arc-discharge method. This method is based on the principle of passing a direct current through two high-purity graphite electrodes (anode and cathode) in different atmospheric gas media (Chen et al. 2012). The synthesis and experimental conditions of graphene are detailed in the previous work by Colak et al. (Colak et al. 2020). Then, the functionalization of the graphene process was started to increase the interface interaction between graphene and epoxy. Triton X-100 was used as a surfactant in this process.

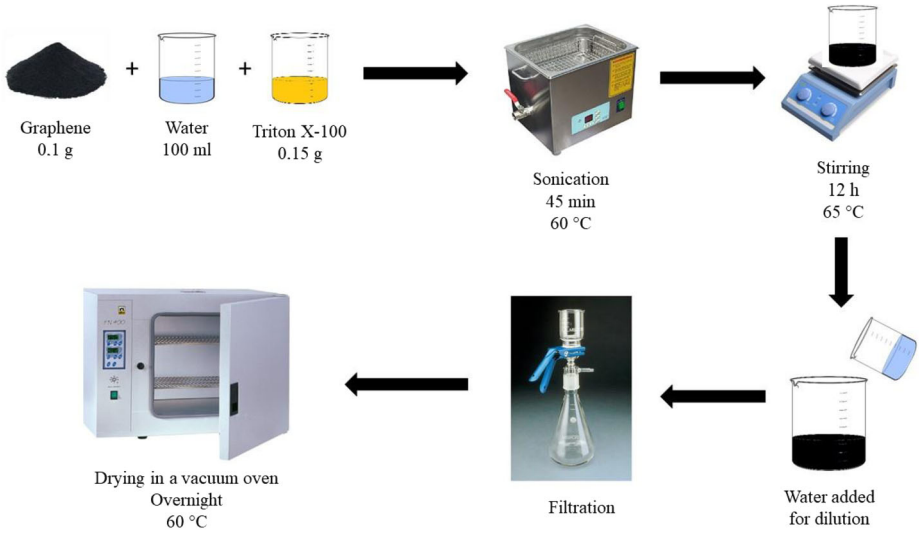

Fig. 1 Functionalization process of graphene

2.2 Functionalization of graphene with triton X-100

For functionalization of graphene, first graphene (0.1 g), purified water (100 ml) and Triton X-100 (POPE) (0.15 g) are mixed in a beaker. Then, the water–graphene–POPE mixture is sonicated for 45 min in a sonic bath at 60 °C. After sonication, the mixture is stirred for 12 h at 65 °C on a magnetic stirrer. After stirring homogeneously, the mixture is filtered using a filter paper (0.45 μm) under vacuum. Lastly, the filtered graphene flakes are dried in a vacuum oven at 60 °C overnight (Fig. 1).

2.3 Manufacturing of f-GNF–epoxy nanocomposite

In this study, the three-roll milling (3RM) method was used as the main strategy to prevent clumping (agglomeration) of graphene. The 3RM method is based on the principle of creating shear stress on the material by using three rollers (feed roller, center roller and apron roller) rotating in opposite directions and at different speeds (Fig. 2). Generally, the material is poured into the feed roller and is subjected to shear stress. Then, the material passing from the central roller to the apron roller is again subjected to much higher shear stresses due to the difference in speed. Finally, the pasty material is collected from the apron roller with the help of a scraper blade. As a result, the material obtained is very well mixed and free from agglomerations. This process can be repeated for several cycles to improve the mixture.

The manufacturing procedure for f-GNF–epoxy nanocomposite is as follows:

For better dispersion in the matrix material (Araldite LY 564), nanocomposite specimens are produced with f-GNF using a three-roll mill (EXACT 80E). Epoxy resin and f-GNF are mixed in a beaker and stirred in a mechanical stirrer for 15 min at 400 rpm. The mixture is calendared for different cycles with a 3RM. The distances between the rollers are kept at 5 μm and the apron speed was 250 rpm for all cycles. After the calendaring, hardener (Aradure 2954) is added, and the mixture is stirred with a magnetic stirrer for 5 min at 400 rpm. The beaker containing the graphene–epoxy mixture is then put into a vacuum chamber

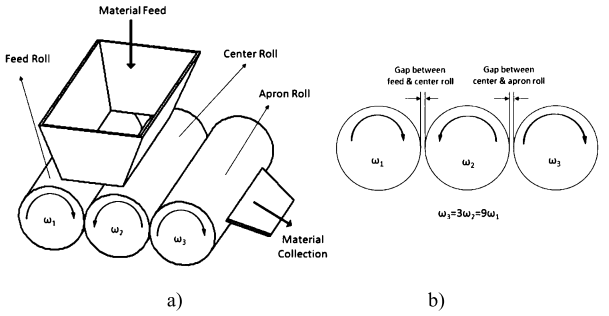

Fig. 2 **a**) Three-roll mill configuration, **b**) High-shear region between the rolls

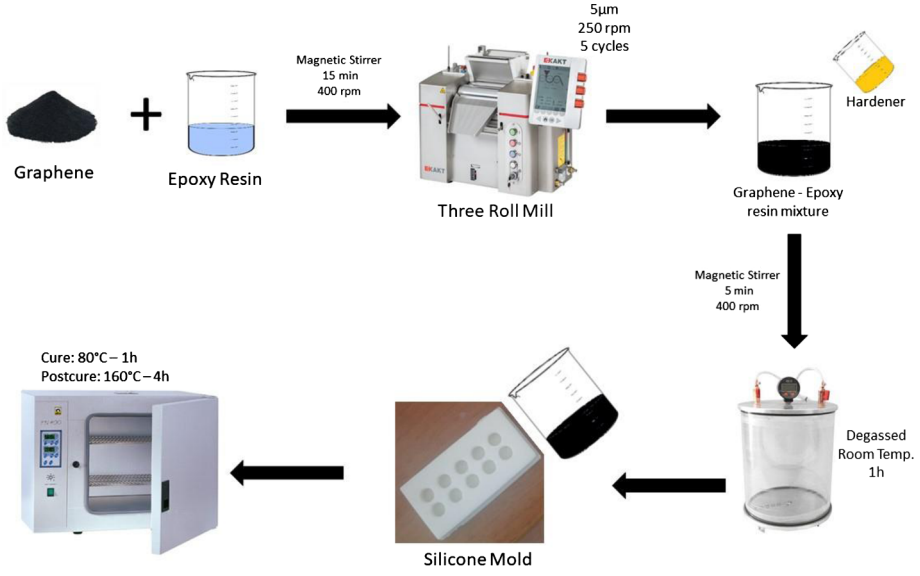

Fig. 3 Production of nanocomposite specimens using 3RM

and degassed for 1 h to eliminate undesired air bubbles. Lastly, the material is poured into soft silicone molds and cured in an oven at 80 °C for 1 h and postcured at 160 °C for 4 h (Fig. 3).

3 Results and discussion

3.1 Determining the optimum number of cycles in 3RM

Homogeneous distribution of graphene in the epoxy is achieved using the three-roll milling method shown in Fig. 3. To ensure a better homogenization, the process of passing the mixture through the rollers is performed for several cycles. The optimum number of cycles was determined by investigating the effect of cycle number on the mechanical properties. During three-roll milling, it is observed that macroclusters of f-GNF (that can be seen with the naked eye inside the matrix material) are not disturbed for the first four cycles. Therefore,

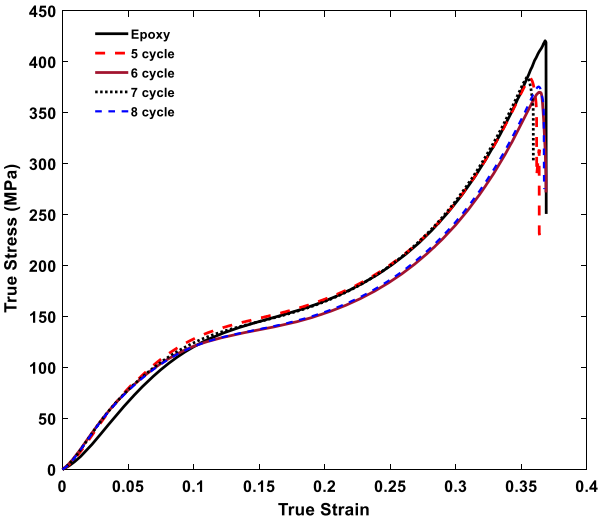

Fig. 4 The true stress–strain curves under compression for various 3RM cycle numbers (Material: GNF–epoxy nanocomposite)

for cycles 2–4 specimens are not produced, since it is obvious that a homogeneous dispersion is not achieved. To optimize the three-roll milling dispersion parameters, initially, the nanocomposite manufactured with the different number of cycles (5–8 cycles) in 3RM has been tested at 1.E-2 /s strain rate. The true stress–strain curves for various cycle numbers are given in Fig. 4.

As can be seen in Fig. 4 the compression behavior of the nanocomposite material produced with different cycle numbers has a similar trend to that of pure epoxy. The material properties (elasticity modulus, yield strength) in the elastic region of the nanocomposite specimens (produced by 0.1 wt% GNF) changed in comparison to the pure epoxy. However, it is observed that the increase in the number of cycles does not provide a significant increase in the mechanical properties of the material. The material behavior of the nanocomposite produced in 3RM with five cycles showed an improvement in the elastic region compared to pure epoxy. It is observed that the material behavior of the specimen produced with five cycles was slightly better than the material behavior of specimens produced with other cycles (6, 7 and 8 cycles). In addition, the increase in the number of cycles increases both the specimen production time and each additional cycle leads to an increase in material waste (material remaining on rolls and in used beakers). Considering all these features, in this study, it was decided to produce nanocomposite specimens with five cycles in the 3RM method.

3.2 Characterization of graphene, f-GNF and dispersion quality

In this study, surface functionalization was performed with Triton X-100 ($C_{14}H_{22}O(C_2H_4O)$ n (n = 9–10)) to improve the interaction of graphene with the epoxy matrix. After the functionalization process, the structural characterization was carried out to investigate the changes in the structure of graphene and f-GNF. The characterization techniques used for this purpose are:

1. Raman spectroscopy;
2. Fourier transform infrared spectroscopy (FT-IR).

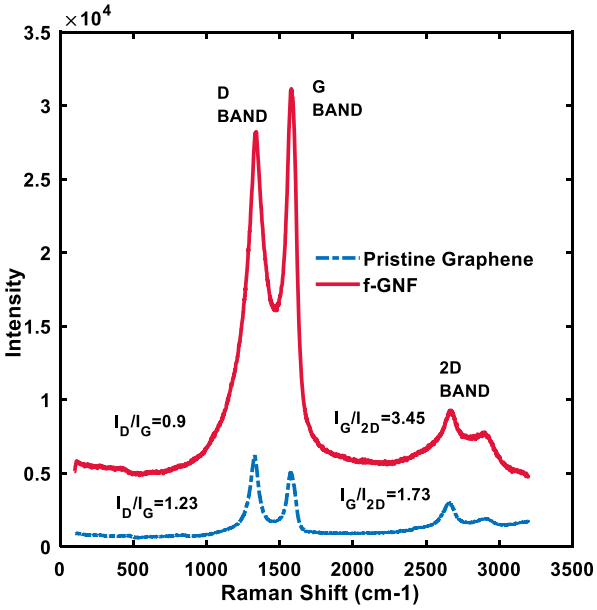

Fig. 5 Raman spectrographs of pristine graphene and f-GNF

In addition, SEM imaging is used to observe the dispersion quality of f-GNF inside the matrix material.

3.2.1 Raman spectroscopy

Raman spectroscopy was performed to investigate the defects and the number of layers of GNF and f-GNF. The results of Raman spectroscopy are given in Fig. 5.

Raman spectroscopy is a characterization method used to investigate the structural and electronic properties of graphene materials. The D band (∼1350 cm^{-1}) shows defects in the structure of carbon-based materials due to lattice distortion caused by impurity elements (Kaykılarlı et al. 2020). The G band (∼1580 cm^{-1}) relates to the sp^2 resonance on an ordered graphitic lattice, and this band position and shape indicate the doping effect. It shows the defects, the number of graphene layers, and the stresses (Kaykılarlı et al. 2020; Zhang et al. 2016). The 2D band (∼2670 cm^{-1}) provides useful information about the stacking order (Ni et al. 2008).

By calculating the ratio of the intensity of the D- and G- Raman peaks (I_D/I_G) in the current Raman plot in Fig. 5, the level of irregularity in the graphene can be characterized (Jang 2013), and this value should be between about 0–1 (Cotul et al. 2018). The ratio of I_G and I_{2D} intensities, (I_G/I_{2D}) gives information about the number of layers of graphene. When this ratio is about 0.25, graphene is a single layer and an increase in ratio indicates an increase in the number of layers (Wu et al. 2010). In the previous studies, the number of layers showed the ratio in the I_G/I_{2D} formula as 0.25 or 0.34. The value resulting from I_G/I_{2D} should be divided by this value (Kaykılarlı et al. 2020; Wu et al. 2010).

Referring to the graphs in the figure of the graphene structure; there are clear, significant peaks. The dotted-lined peaks indicate pristine graphene (collected from the arc reactor directly from the anode zone), and the solid line indicates surface-functionalized graphene with Triton X-100. Raman values in the resulting graphic occur between 1250 cm^{-1} and 2750 cm^{-1} for both material types. D, G and 2D bands of pristine graphene (taken from

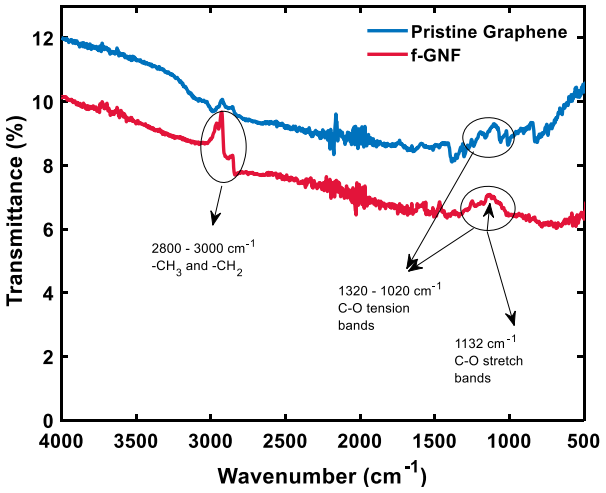

Fig. 6 FT-IR results of pristine graphene and f-GNF

the reactor) are located at values of 1328 cm^{-1}, 1575 cm^{-1} and 2661 cm^{-1}, respectively. Its purity was calculated as 1.23, from the I_D/I_G ratio. The number of layers is between 5 and 7 from the I_G/I_{2D} ratio. For f-GNF, the D, G and 2D bands are positioned at 1340 cm^{-1}, 1579 cm^{-1} and 2672 cm^{-1}, respectively. The Raman values of f-GNF are calculated as 0.9 from the I_D/I_G ratio; the number of layers is between 10 and 13.

As a result, both the purity and the number of layers of f-GNF increase significantly. The number of layers increased almost twofold compared to pristine graphene. The reason for the low purity (defect rate) of pristine graphene is the increase in the number of defects and edges in the cage during exfoliation (multilayer graphene also supports this view). Carrasco et al. explain the increase in density as the effect of Triton X-100 on the surface of the graphene (Carrasco et al. 2014). The reason why the G bands of pristine graphene and f-GNF are aligned is that graphene does not have any double bonds after it becomes functional (as the peaks of graphite oxide (GO) and graphite are not aligned because of the presence of double bonds in GO) (Kudin et al. 2008).

3.2.2 Fourier transform infrared spectroscopy (FT-IR)

Fourier transform infrared spectroscopy (FT-IR) was performed to investigate the molecular orientation and types of bonds and molecules of GNF and f-GNF. The results of FT-IR are given in Fig. 6. FT-IR spectra provide information about the molecular orientation of the polymeric-based graphene structure (Qamar et al. 2019). The spectrometer is based on the principle of the absorption of infrared rays. Infrared rays only apply the absorption process that occurs between variable dipole-bound molecules. Its principle is similar to Raman spectroscopy, but it differs in the basis of the measurements of graphene-based materials due to its results (it is generally used in the determination of organic materials such as C, H, O, N).

FT-IR spectra were measured on a Nicolet FT-IR spectrophotometer (Nicolet IS510, Nicolet Instrument Company, Madison, WI, USA) with a resolution of 2 cm^{-1} between 500 and 4000 cm^{-1}. Two specimens consisting of GNF and f-GNF were tested, respectively. Both specimens were pressed during the test.

The peaks indicate particularly carbonyl and benzene carboxyl groups through vibrations created by molecules and bonds (Qamar et al. 2019). Figure 6 shows that the Triton X-100

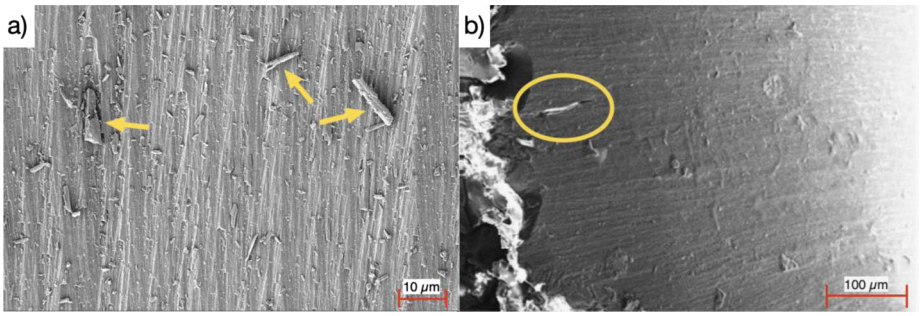

Fig. 7 **a**) 0.5 wt% f- GNF–epoxy nanocomposite; **b**) images of the fractured surfaces of pure epoxy at 500× zoom

surfactant can be physically adsorbed at the surface of GNF via hydrophobic segments. In contrast to the pristine GNF, the TX-100-treated GNF sample (f-GNF) obviously shows the presence of methylene and methyl groups. Peaks at 1320–1020 cm^{-1}, which are adsorbed through hydrophobic segments on the surface of GNF, are ascribed to C–O tension bands that reflect Triton X-100 molecules (Li et al. 2014). It is possible to note the aromatic C–H structures due to vibration and interaction in the f-GNF peaks (Geng et al. 2008). In the f-GNF spectrum, the peaks at 1132 cm^{-1} correspond to C–O stretch bands. Absorption peaks at 2800 cm^{-1} and 3000 cm^{-1} are probably based on symmetric and asymmetric stress vibration of the $-CH_3$ and $-CH_2$ groups from Triton X-100. This vibration shows that Triton X-100 molecules and bonds are adsorbed on the surface of GNF, as shown in Fig. 6 (Li et al. 2014; Wan et al. 2013). The mentioned peaks, unlike the insignificant peaks in the pristine spectrum, confirm GNF functionalization. The presence of high-intensity sp^3-carbons in the TX-100 led to adsorption of more surfactant clusters on the GNF surface, these clusters increased the oxygenated functional groups (Mohd Amran et al. 2021).

3.2.3 Investigation of dispersion state through scanning electron microscopy (SEM)

Figure 7 shows SEM images of fracture surfaces of pure epoxy and f-GNF–epoxy composites with 500× magnification. Unlike the fracture surfaces of pure epoxy resin, the surfaces of nanocomposites are rough. Due to the two-dimensional (2D) structure of graphene nanoplates, it effectively distorts and deflects crack propagation (Wang et al. 2013). The surface roughness of nanocomposites is clearly higher than the surface roughness of pure epoxy. Defects on nanocomposites are divided into deep and shallow cracks. The pattern of deep cracks is quite similar to pure-epoxy specimens. However, the density of shallow cracks in nanocomposites is relatively much higher, which can be explained by the pressure of f-GNFs inside the matrix of the nanocomposite. In fact, the f-GNF particles cause the change in the direction of the fracture plane and create rifts (Shadlou et al. 2014).

The drawn arrows and oval indicate the surface roughness and the size of cracks, respectively. After testing, the surface of the nanocomposite is expected to be rougher and large cracks are seen in pure epoxy.

3.3 Mechanical characterization of f-GNF–epoxy nanocomposite

Three different types of tests were carried out for the experimental investigation of the viscoelastic response. These are compression tests at different strain rates, creep and stress-relaxation tests.

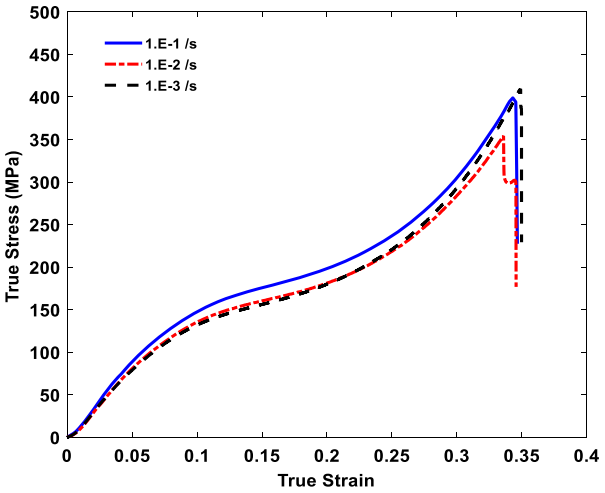

Fig. 8 True stress–strain behaviors of f-GNF–epoxy nanocomposites with f-GNF content of 0.1 wt% at three different strain rates

3.3.1 Quasistatic compression tests

To investigate the viscoelastic and viscoplastic behavior of epoxy and f-GNF–epoxy nanocomposites, quasistatic compression tests at different strain rates were performed on an INSTRON 5982 universal test device. The cylindrical specimens used in the compression test are 12 mm in diameter and length. Compression tests of pure epoxy (Araldite LY 564) and f-GNF–epoxy nanocomposites (f-GNF content of 0.1 and 0.5 wt%) were conducted at room temperature for three different strain rates (1.E-3, 1.E-2 and 1.E-1 /s). To guarantee the repeatability of the test results, three specimens were tested for all strain rates and the mean results are reported. It is observed that the repeatability of the tests is good, due to overlapped results. Tests are performed in strain-control mode, i.e., the displacement of the crosshead is increased at a constant rate with increasing time, and the corresponding force values are recorded. The true stress–strain behaviors of f-GNF–epoxy nanocomposites with contents of f-GNF of 0.1 and 0.5 wt% at three different strain rates are depicted in Figs. 8 and 9, respectively.

As can be seen from Figs. 8 and 9, the change in material behavior of nanocomposites (containing 0.1 and 0.5 wt% f-GNF) follows a similar trend at all three strain rates. As the strain rate increases, the elasticity modulus and yield strength of the nanocomposite materials increase. The elasticity modulus is determined as the slope in the viscoelastic linear region. The viscoelastic region of the f-GNF–epoxy nanocomposite is the part up to the point where the material starts to yield. The linear zone of deformation is referred to as viscoelastic but not elastic, since the material response changes with changing strain rate. The point where linearity ends and nonlinearity begins is determined as the yield strength. That is, the point where the slope of the stress–strain curve is zero for the first time is the yield stress. The point where strain-softening behavior begins after the material reaches its yield strength is accepted as the beginning of the viscoplastic region (Bakbak et al. 2021; Colak and Cakir 2019). There is a linear increase in the viscoelastic region from the first loading and rate dependency is quite minimal in this region. This situation is understood by the limited increase in the elasticity modulus. In the material behavior of f-GNF–epoxy nanocomposites, a rate-dependent yield region after viscoelastic behavior followed by an insignificant strain softening and a pronounced nonlinear hardening in the viscoplastic region

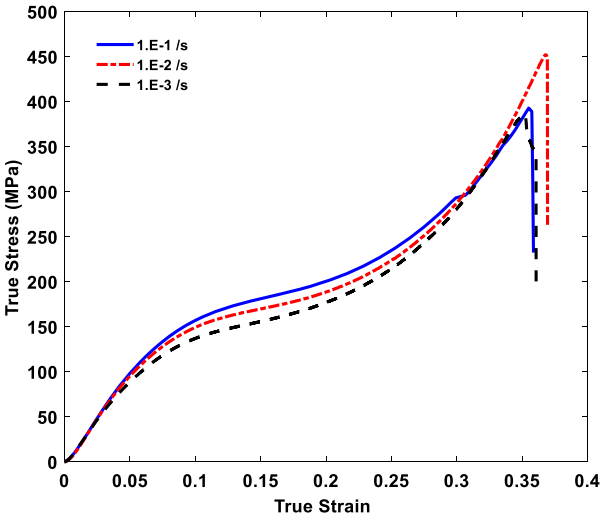

Fig. 9 True stress–strain behaviors of f-GNF–epoxy nanocomposites with f-GNF content of 0.5 wt% under three different strain rates

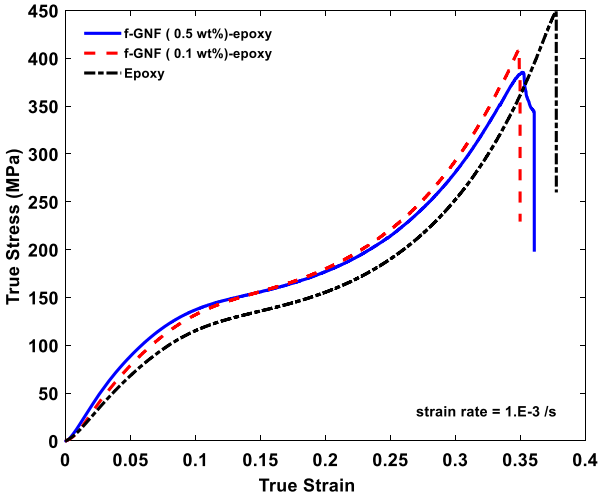

Fig. 10 Comparison of true stress–strain behaviors of f-GNF–epoxy nanocomposites with f-GNF content of 0.1 and 0.5 wt% with pure epoxy at 1.E-3 /s strain rate. Experimental data about epoxy are taken from (Bakbak et al. 2021)

is observed. Rate dependency in the viscoplastic region is more prominent than it is in the viscoelastic region. As the strain rate increases, the improvement in material properties can be explained by the restriction of the movement of the polymer chains that results in a stiffer material response.

The true stress–strain behavior of f-GNF–epoxy nanocomposites with contents of 0.1 and 0.5 wt% f-GNF compared to pure epoxy at three different strain rates for 1.E-3, 1.E-2, 1.E-1 /s, are shown in Figs. 10–12, respectively. The test results for pure epoxy are taken from a previous study of our research group (Bakbak et al. 2021).

It is observed that the material behavior of nanocomposites obtained by adding f-GNF to the epoxy at all strain rates improves compared to pure epoxy in both the viscoelastic and viscoplastic regions (Figs. 10, 11, 12). Elasticity modulus and yield strength of f-GNF–epoxy nanocomposites containing different amounts of f-GNF increased compared to epoxy at all strain rates. The elasticity modulus and yield strength of pure epoxy and

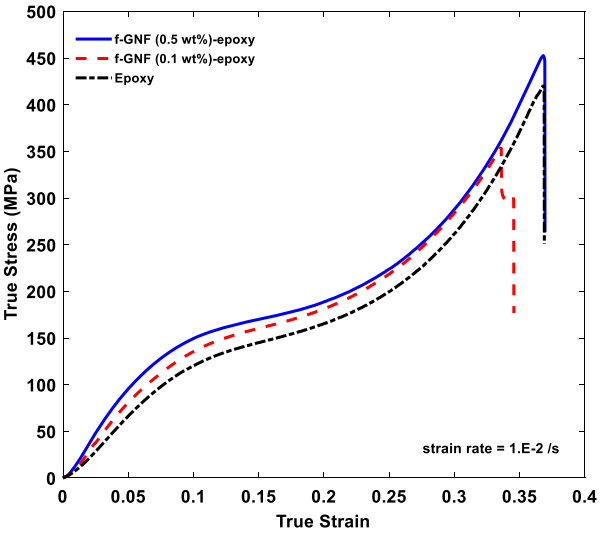

Fig. 11 Comparison of true stress–strain behaviors of f-GNF–epoxy nanocomposites with f-GNF content of 0.1 and 0.5 wt% with pure epoxy at 1.E-2 /s strain rate. Experimental data about epoxy are taken from (Bakbak et al. 2021)

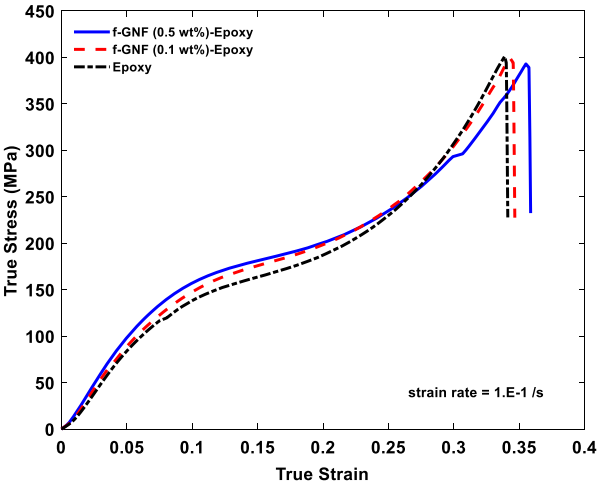

Fig. 12 Comparison of true stress–strain behaviors of f-GNF–epoxy nanocomposites with f-GNF content of 0.1 and 0.5 wt% with pure epoxy at 1.E-1 /s strain rate. Experimental data about epoxy are taken from (Bakbak et al. 2021)

f-GNF nanocomposites are shown in Table 1. This table also shows the increase in material properties as percentages for different graphene concentrations and strain rates.

In the relevant literature, it is reported that enhancements in the mechanical properties of nanocomposites are limited to a certain graphene concentration, which is around 0.1 wt%, but when this level is exceeded, the mechanical properties are decreased due to agglomeration and weak interface-bonding problems (Acar et al. 2015; Colak et al. 2020; Poutrel et al. 2017; Zandiatashbar et al. 2012). However, in this study, as can be seen in Figs. 10–12 and Table 1, the improvement in material properties continued to rise above this concentration level. This improvement is explained by the functionalization of graphene with Triton X-100 and effectively dispersing graphene in the epoxy matrix using the 3RM method.

The functionalization of graphene surfaces with a surfactant significantly improves its dispersion in the matrix material and provides efficient interface interaction with the matrix material (Wan et al. 2013). In this study, Triton X-100, a nonionic surfactant used to

Table 1 Mechanical properties of pure epoxy (Bakbak et al. 2021) and f-GNF–epoxy nanocomposite (0.1 and 0.5 wt% f-GNF) obtained from the quasistatic compression test

Mechanical properties	Strain rate (1/s)	Pure epoxy	f-GNF–epoxy (0.1 wt%)	f-GNF–epoxy (0.5 wt%)	Change (%) (0.1 wt% nanocomposite–pure epoxy)	Change (%) (0.5 wt% nanocomposite–pure epoxy)	Change (%) (0.1 wt% nanocomposite–0.5 wt% nanocomposite)
Elasticity Modulus (MPa)	1.E-1	1987	2104	2237	6	11	6
	1.E-2	1542	1899	2171	19	29	13
	1.E-3	1465	1878	2063	22	29	9
Yield strength (MPa)	1.E-1	137	153	162	10	15	6
	1.E-2	124	142	151	13	18	6
	1.E-3	119	134	138	11	14	3

functionalize graphene, contains hydrophilic and hydrophobic groups, and the hydrophobic groups are effective in the homogeneous dispersion of graphene by adsorbing onto graphene surfaces (Wan et al. 2013). The hydrophilic groups of Triton X-100 also interact with the matrix material through hydrogen bonding and thus this surfactant acts as a bridge between graphene and epoxy (Poutrel et al. 2017). As a result, both the graphene dispersion becomes more effective, and the interface interaction between the matrix material and graphene increases. Another factor that improves mechanical properties is the production of nanocomposites with the 3RM method. With the effect of shear stress in this method, the agglomeration problem was prevented by breaking the van der Waals bonds in graphene. As a result, as can be seen from Table 1, the highest improvements in both elasticity modulus and yield strength compared to pure epoxy are observed for 0.5 wt% f-GNF composites at all strain rates.

The above well-defined and the experimentally characterized reinforcing mechanism is effective for strain values smaller than $\cong 0.25$, as can be seen from Figs. 10–12. At large strain values, the graphene flakes are found to be completely or partially debonded from the epoxy matrix, and act like voids and weaken the composite material. Similar theoretical results are reported by Tan et al. for carbon nanotube–polymer interfacial bonds (Tan et al. 2007).

3.3.2 Creep experiments at different stress levels

The time-dependent mechanical behavior of the nanocomposites is investigated by creep and stress-relaxation tests. In order to assess the effect of GNF in the epoxy matrix, the results are compared to the results for pure epoxy reported by Bakbak et al. (Bakbak et al. 2021).

Creep-stress levels are selected in such a way that the behaviors at the viscoelastic region and around the yield region can be investigated. These stress levels are 50 and 100 MPa. Creep tests were performed at a strain rate of 1.E-1/ s and under compression mode and for 7200 s at room temperature. Three tests are performed for f-GNF–epoxy nanocomposites under each constant stress level and the mean results are reported. The repeatability of the tests is observed to be reasonably good. Changes in the creep strain versus time at 50 and 100 MPa stress levels are presented in Figs. 13 and 14, respectively. The data obtained from the creep tests are shown in Tables 2 and 3.

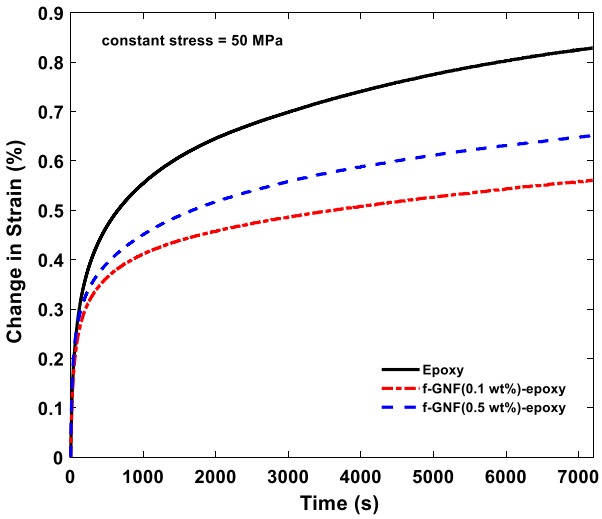

Fig. 13 Change in creep strain versus time response for creep tests at 50 MPa stress level. Experimental data about epoxy are taken from Bakbak et al. (Bakbak et al. 2021)

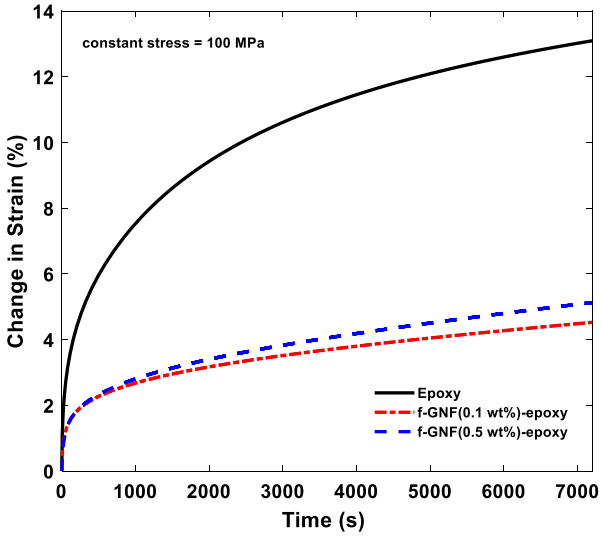

Fig. 14 Change in creep strain versus time response for creep tests at 100 MPa stress level Experimental data about epoxy are taken from Bakbak et al. (Bakbak et al. 2021)

As seen in Figs. 13 and 14, the creep strain increases for both concentrations as the strain level changes from 50 to 100 MPa. In the viscoelastic region, i.e., at the 50-MPa stress level, the time dependence is low, as explained in Sect. 3.3.1. However, at the 100-MPa stress level, which is close to the yield region, epoxy chains shift relative to each other more freely, therefore the creep strain increases (Bakbak et al. 2021). When the creep behavior of nanocomposites is compared to pure epoxy (Bakbak et al. 2021), it is seen that the creep strain of nanocomposites at both stress levels is lower than that of pure epoxy (Table 2). Similar results are reported in the relevant literature (Tang et al. 2014; Wang et al. 2015b; Yang et al. 2007; Zandiatashbar et al. 2012; Zhang et al. 2007). As seen in Table 3, an improvement in creep-strain data is observed with the addition of f-GNF. At the 50-MPa stress level, the decrease in creep strain (i.e., increase in creep resistance) with the addition

Table 2 Data obtained from the creep test at 2 different stress levels (50 and 100 MPa)

Material	Constant stress (MPa)	Creep strain ($t = 1$ s)	Creep strain ($t =$ 7200 s)	Change in creep strain (%) (at end of creep test)
Pure epoxy (Bakbak et al. 2021)	50	0.04054	0.04883	0.829
0.1 wt% f-GNF–epoxy	50	0.03445	0.04006	0.561
0.5 wt% f-GNF–epoxy	50	0.02877	0.03528	0.651
Pure epoxy (Bakbak et al. 2021)	100	0.09072	0.22167	13.095
0.1 wt% f-GNF–epoxy	100	0.07447	0.11971	4.524
0.5 wt% f-GNF–epoxy	100	0.07798	0.12924	5.124

Table 3 Improvement of nanocomposites compared to pure epoxy (Bakbak et al. 2021)

Material	Decrease in creep strain compared to epoxy (%)
0.1 wt% f-GNF–epoxy (50 MPa)	32.32
0.5 wt% f-GNF–epoxy (50 MPa)	21.47
0.1 wt% f-GNF–epoxy (100 MPa)	65.45
0.5 wt% f-GNF–epoxy (100 MPa)	60.85

of 0.1 and 0.5 wt% f-GNF is 32.32 and 21.47%, respectively, while at the 100-MPa stress level it is 65.45 and 60.85%, respectively. As seen from Figs. 13 and 14, at the low stress level (50 MPa), the influence of nanofiller weight fraction on creep strain is much more prominent than that at the higher stress level (100 MPa). The increase in creep resistance can be explained by the mechanism that f-GNF, which is the reinforcing element, prevents the movement of epoxy chains by acting as a barrier. The strong interfacial interaction of f-GNF with epoxy and the dispersing of f-GNF homogeneously in the epoxy matrix is of course critical to this improvement.

As can be seen from Figs. 13 and 14 and Tables 2 and 3, the 0.1 wt% f-GNF concentration has a larger effect on creep behavior when compared to 0.5 wt%. While the mechanical properties such as strength, stiffness and toughness of graphene-reinforced epoxy nanocomposites have been extensively investigated, the research on creep behaviors showing the long-term performance of these materials is still quite limited and not adequately understood. Understanding of the creep deformation and the reinforcing mechanism of creep resistance in nanocomposites at the atomistic level is still needed (Jian and Lau 2019). Creep response is fundamentally related to the change of molecular mobility in polymeric systems. Due to the viscoelastic nature of polymers, the epoxy matrix undergoes time-dependent deformation. The irreversible disentanglement of polymer chains including slippage and stretching, takes place over time (Jian and Lau 2019). During creep deformation, the chain reorientation in the polymer matrix is induced by the external stress, and the molecular motion is changed over time. There is a strong correlation between the molecular mobility and the strain rate (Lee et al. 2009).

Creep experiments on graphene or carbon nanotubes (CNTs)-reinforced epoxy nanocomposites yield inconsistent conclusions on whether the addition of nanofiller can greatly improve the creep resistance of nanocomposites or not. At higher weight fraction and creep loads, the reinforcing ability of graphene and CNTs in nanocomposites is weaker as agglomeration occurs. In such cases, the adhesion between nanofiller and epoxy matrix deteriorates.

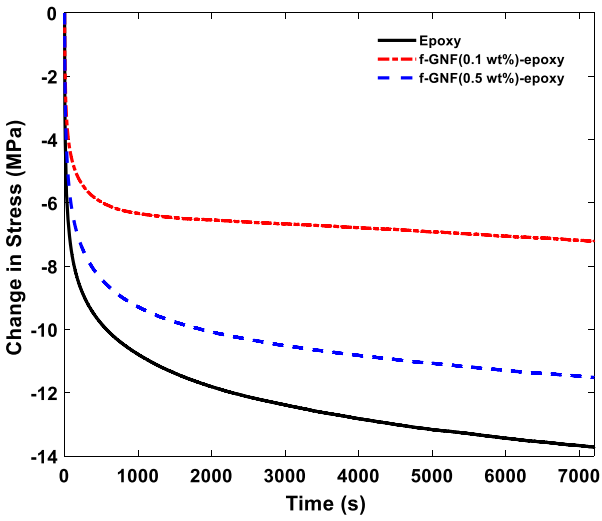

Fig. 15 Change in stress versus time response during relaxation tests at a 3.16% strain level. Experimental data of epoxy are taken from Bakbak et al. (Bakbak et al. 2021)

In contrast, increasing nanofiller weight fraction with good dispersion results in a noticeable decrease of creep strain (Jian and Lau 2019; Papanicolaou et al. 2012). Such a discrepancy in experimental findings is caused by various fabrication factors, indicating the dependency of the creep resistance on nanofiller size, weight fraction and state of dispersion.

Since there are limitations in the precise control of parameters, it is insufficient to explain the effect of individual parameter on the segmental dynamics in an epoxy matrix solely by experiments. Therefore, the investigation from the nanoscale perspective can help to uncover the microstructural interactions and dynamics in the graphene–epoxy nanocomposites, enabling the analysis of the effects from different graphene-associated parameters (Khabaz-Aghdam et al. 2020).

3.3.3 Stress-relaxation experiments at different strain levels

In stress-relaxation experiments, the compression specimen is subjected to a constant displacement load and the change of stress is monitored using Instron 5982 universal testing equipment. The stress-relaxation tests were conducted at 3.16% strain (corresponds to ≈50 MPa on the compression curve) and 7.15% strain (corresponds to ≈100 MPa on the compression curve); for 7200 s for all specimens (with contents of 0.1 and 0.5 wt% f-GNF). Compression loading up to the strain levels mentioned above is performed at a strain rate of 1.E-1/s. Changes in the stress–time graphs are shown in Figs. 15 and 16 for two different strain levels. Stress-relaxation test results are given in Table 4.

As seen from Fig. 16 and Table 4, the addition of f-GNF improved the stress-relaxation behavior as well. Stress-drop levels are lower when compared to pure epoxy results from Bakbak et al. (Bakbak et al. 2021). At a 3.16% constant strain level with the addition of 0.1 and 0.5 wt% f-GNF 17.7 and 22.7% stress drops are observed, respectively, while at a 7.15% constant strain level stress drop values are observed as 22.1 and 25.5%, respectively (Table 4). This result can also be explained by obstruction of polymer-chain movements by graphene flakes, as seen in the creep results. Stress-relaxation behavior is more prominent in the yield region when compared to the viscoelastic region, as seen in the creep behavior. This result also supports the hypothesis that was stated for the creep-test results: the time dependence is more prominent in the yield region.

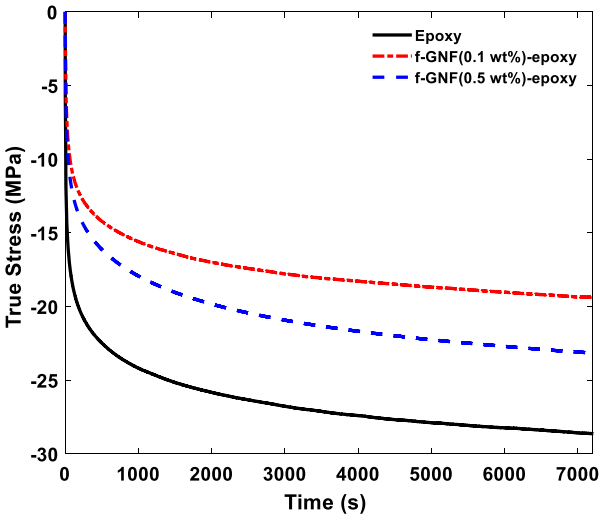

Fig. 16 Change in stress versus time response during relaxation tests at a 7.15% strain level. Experimental data of epoxy are taken from Bakbak et al. (Bakbak et al. 2021)

Table 4 Stress drop values during relaxation tests

Constant Strain (%)	Material	Stress drop (MPa)	Stress drop (%)
3.16	Pure epoxy (Bakbak et al. 2021)	13.71	25.9
	0.1 wt% f-GNF–epoxy	7.21	17.7
	0.5 wt% f-GNF–epoxy	11.51	22.7
7.15	Pure Epoxy (Bakbak et al. 2021)	28.62	31.8
	0.1 wt% f-GNF–epoxy	19.36	22.1
	0.5 wt% f-GNF–epoxy	23.14	25.5

4 Conclusions

Graphene–epoxy nanocomposites are prepared for two different graphene fractions, 0.1 and 0.5 wt%. 3RM is used as the main strategy for a homogeneous dispersion of graphene in the epoxy matrix. In order to determine the optimum number of cycles of 3RM, nanocomposite materials are prepared, and nanocomposites are subjected to compression tests. No significant difference is observed for 5–8 cycles, on the compression behavior. Only a slight decrease in the yield stress is observed for cycle numbers higher than five.

Functionalization of GNFs using Triton X-100 as a surfactant is performed to improve the interfacial bonding between matrix and graphene, and also to prevent agglomeration. The effectiveness of the functionalization procedure is investigated using Raman spectroscopy and FT-IR. The results showed that the Triton X-100 is adsorbed on the surface of GNFs.

The produced nanocomposites are subjected to compression tests at three different strain rates (1.E-1, 1.E-2 and 1.E-3 /s). As expected, higher modulus and yield-strength values are observed as the strain rate increases. The results of nanocomposites are compared to pure-epoxy compression test results from Bakbak et al. (Bakbak et al. 2021); up to 29% increase in elasticity modulus and up to 18% increase in yield strength is achieved with the addition of 0.5 wt% graphene. In the relevant literature, for nanocomposite materials that have graphene contents greater than 0.1 wt%, the mechanical properties start to deteriorate,

due to agglomeration and poor load transfer from graphene to the matrix. In this work, this problem is overcome using functionalization with Triton X-100 and using 3RM as the dispersing strategy; almost all values for 0.5 wt% graphene nanocomposites are higher than those of 0.1 wt%.

In order to propose a total viscoelastic characterization, creep tests at two different stress levels (50 and 100 MPa) and stress-relaxation tests at two corresponding strain levels are performed. The results of creep and stress-relaxation tests are compared to pure-epoxy test results from Bakbak et al. (Bakbak et al. 2021). Compared to the creep behavior of epoxy, 32% and 65% less creep strain is observed at 0.1 wt% f-GNF–epoxy at 50 and 100 MPa, respectively. Stress-relaxation behavior is also improved with the addition of functionalized graphene.

Therefore, it is shown that the three-roll milling and functionalization procedure that is used in this work is highly efficient to achieve a homogeneous dispersion of GNFs inside the epoxy matrix, and therefore an effective load transfer between graphene and matrix material, which yields improved mechanical properties.

Acknowledgements We thank Ozberk Oztürk for performing Raman spectra and FT-IR tests.
Funding: This work is supported by TUBİTAK. Project number: 119M088.

Data Availability Data will be made available on reasonable request.

References

Acar, A., Çolak, Ö.Ü., Uzunsoy, D.: Synthesis and characterization of graphene-epoxy nanocomposites. Mater. Test. **57**, 1001–1005 (2015). https://doi.org/10.3139/120.110804

Ahmadi-Moghadam, B., Taheri, F.: Effect of processing parameters on the structure and multi-functional performance of epoxy/GNP-nanocomposites. J. Mater. Sci. **49**, 6180–6190 (2014). https://doi.org/10.1007/s10853-014-8332-y

Anwer, M.A.S., Wang, J., Naguib, H.E.: 1D/2D CNF/GNP hybrid nanofillers: evaluation of the effect of surfactant on the morphological, mechanical, fracture, and thermal characteristics of their nanocomposites with epoxy resin. Ind. Eng. Chem. Res. **58**, 8131–8139 (2019). https://doi.org/10.1021/acs.iecr.9b00956

Bakbak, O., Birkan, B.E., Acar, A., Colak, O.: Mechanical characterization of Araldite LY 564 epoxy: creep, relaxation, quasi-static compression and high strain rate behaviors. Polym. Bull. (2021). https://doi.org/10.1007/s00289-021-03624-x

Balandin, A.A., Ghosh, S., Bao, W., Calizo, I., Teweldebrhan, D., Miao, F., Lau, C.N.: Superior thermal conductivity of single-layer graphene. Nano Lett. **8**, 902–907 (2008). https://doi.org/10.1021/nl0731872

Carrasco, P.M., Montes, S., García, I., Borghei, M., Jiang, H., Odriozola, I., Cabañero, G., Ruiz, V.: High-concentration aqueous dispersions of graphene produced by exfoliation of graphite using cellulose nanocrystals. Carbon **70**, 157–163 (2014). https://doi.org/10.1016/j.carbon.2013.12.086

Chandrasekaran, S., Seidel, C., Schulte, K.: Preparation and characterization of graphite nano-platelet (GNP)/epoxy nano-composite: mechanical, electrical and thermal properties. Eur. Polym. J. **49**, 3878–3888 (2013). https://doi.org/10.1016/j.eurpolymj.2013.10.008

Chandrasekaran, S., Sato, N., Tölle, F., Mülhaupt, R., Fiedler, B., Schulte, K.: Fracture toughness and failure mechanism of graphene based epoxy composites. Compos. Sci. Technol. **97**, 90–99 (2014). https://doi.org/10.1016/j.compscitech.2014.03.014

Chen, Y., Zhao, H., Sheng, L., Yu, L., An, K., Xu, J., Ando, Y., Zhao, X.: Mass-production of highly-crystalline few-layer graphene sheets by arc discharge in various H2–inert gas mixtures. Chem. Phys. Lett. **538**, 72–76 (2012). https://doi.org/10.1016/j.cplett.2012.04.020

Colak, O.U., Cakir, Y.: Material model parameter estimation with genetic algorithm optimization method and modeling of strain and temperature dependent behavior of epoxy resin with cooperative-VBO model. Mech. Mater. **135**, 57–66 (2019). https://doi.org/10.1016/j.mechmat.2019.04.023

Colak, Ö.U., Bahlouli, N., Uzunsoy, D., Francart, C.: High strain rate behavior of graphene-epoxy nanocomposites. Polym. Test. **81**, 106219 (2020). https://doi.org/10.1016/j.polymertesting.2019.106219

Cotul, U., Parmak, E.D.S., Kaykilarli, C., Saray, O., Colak, O., Uzunsoy, D.: Development of high purity, few-layer graphene synthesis by electric arc discharge technique. Acta Phys. Pol. A **134**, 289–291 (2018). https://doi.org/10.12693/APhysPolA.134.289

Dai, J., Peng, C., Wang, F., Zhang, G., Huang, Z.: Effects of functionalized graphene nanoplatelets on the morphology and properties of phenolic resins. J. Nanomater. **2016**, 1–7 (2016). https://doi.org/10.1155/2016/3485167

Geng, Y., Liu, M.Y., Li, J., Shi, X.M., Kim, J.K.: Effects of surfactant treatment on mechanical and electrical properties of CNT/epoxy nanocomposites. Composites, Part A, Appl. Sci. Manuf. **39**, 1876–1883 (2008). https://doi.org/10.1016/j.compositesa.2008.09.009

Georgakilas, V., Tiwari, J.N., Kemp, K.C., Perman, J.A., Bourlinos, A.B., Kim, K.S., Zboril, R.: Noncovalent functionalization of graphene and graphene oxide for energy materials, biosensing, catalytic, and biomedical applications. Chem. Rev. **116**, 5464–5519 (2016). https://doi.org/10.1021/acs.chemrev.5b00620

Hashim, U.R., Jumahat, A.: Improved tensile and fracture toughness properties of graphene nanoplatelets filled epoxy polymer via solvent compounding shear milling method. Mater. Res. Express **6**, 025303 (2018). https://doi.org/10.1088/2053-1591/aaeaf0

Imran, K.A., Shivakumar, K.N.: Enhancement of electrical conductivity of epoxy using graphene and determination of their thermo-mechanical properties. J. Reinf. Plast. Compos. **37**, 118–133 (2018). https://doi.org/10.1177/0731684417736143

Jang, J.I.: New Developments in Photon and Materials Research. Nova Science Publishers, Incorporated, ??? (2013)

Jian, W., Lau, D.: Creep performance of CNT-based nanocomposites: a parametric study. Carbon **153**, 745–756 (2019). https://doi.org/10.1016/j.carbon.2019.07.069

Kaykılarlı, C., Uzunsoy, D., Parmak, E.D.Ş., Fellah, M.F., Çakır, Ö.Ç.: Boron and nitrogen doping in graphene: an experimental and density functional theory (DFT) study. Nano Express **1**, 010027 (2020). https://doi.org/10.1088/2632-959X/ab89e9

Khabaz-Aghdam, A., Behjat, B., da Silva, L.F.M., Marques, E.A.S.: A new theoretical creep model of an epoxy-graphene composite based on experimental investigation: effect of graphene content. J. Compos. Mater. **54**, 2461–2472 (2020). https://doi.org/10.1177/0021998319895806

Kudin, K.N., Ozbas, B., Schniepp, H.C., Prud'homme, R.K., Aksay, I.A., Car, R.: Raman spectra of graphite oxide and functionalized graphene sheets. Nano Lett. **8**, 36–41 (2008). https://doi.org/10.1021/nl071822y

Lee, H.-N., Paeng, K., Swallen, S.F., Ediger, M.D.: Direct measurement of molecular mobility in actively deformed polymer glasses. Science **323**, 231–234 (2009). https://doi.org/10.1126/science.1165995

Li, Q., Church, J.S., Kafi, A., Naebe, M., Fox, B.L.: An improved understanding of the dispersion of multi-walled carbon nanotubes in non-aqueous solvents. J. Nanopart. Res. **16**, 2513 (2014). https://doi.org/10.1007/s11051-014-2513-0

Li, Y., Tang, J., Huang, L., Wang, Y., Liu, J., Ge, X., Tjong, S.C., Li, R.K.Y., Belfiore, L.A.: Facile preparation, characterization and performance of noncovalently functionalized graphene/epoxy nanocomposites with poly(sodium 4-styrenesulfonate). Composites, Part A, Appl. Sci. Manuf. **68**, 1–9 (2015). https://doi.org/10.1016/j.compositesa.2014.09.016

Malysheva, G.V., Akhmetova, E.S., Marycheva, A.N.: Estimation of glass transition temperature of polysulfone-modified epoxy binders. Glass Phys. Chem. **40**, 543–548 (2014). https://doi.org/10.1134/S1087659614050095

Martin-Gallego, M., Yuste-Sanchez, V., Sanchez-Hidalgo, R., Verdejo, R., Lopez-Manchado, M.A.: Epoxy nanocomposites filled with carbon nanoparticles. Chem. Rec. **18**, 928–939 (2018). https://doi.org/10.1002/tcr.201700095

McAllister, M.J., Li, J.-L., Adamson, D.H., Schniepp, H.C., Abdala, A.A., Liu, J., Herrera-Alonso, M., Milius, D.L., Car, R., Prud'homme, R.K., Aksay, I.A.: Single sheet functionalized graphene by oxidation and thermal expansion of graphite. Chem. Mater. **19**, 4396–4404 (2007). https://doi.org/10.1021/cm0630800

Mohd Amran, N.A., Ahmad, S., Chen, R.S., Shahdan, D., Flaifel, M.H., Omar, A.: Assessment of mechanical and electrical performances of polylactic acid/liquid natural rubber/graphene platelets nanocomposites in the light of different graphene platelets functionalization routes. Macromol. Chem. Phys. **222**, 2100185 (2021). https://doi.org/10.1002/macp.202100185

Moriche, R., Prolongo, S.G., Sánchez, M., Jiménez-Suárez, A., Sayagués, M.J., Ureña, A.: Morphological changes on graphene nanoplatelets induced during dispersion into an epoxy resin by different methods. Composites, Part B, Eng. **72**, 199–205 (2015). https://doi.org/10.1016/j.compositesb.2014.12.012

Ni, Z., Wang, Y., Yu, T., Shen, Z.: Raman spectroscopy and imaging of graphene. Nano Res. **1**, 273–291 (2008). https://doi.org/10.1007/s12274-008-8036-1

Papanicolaou, G.C., Xepapadaki, A.G., Drakopoulos, E.D., Papaefthymiou, K.P., Portan, D.V.: Interphasial viscoelastic behavior of CNT reinforced nanocomposites studied by means of the concept of the hybrid viscoelastic interphase. J. Appl. Polym. Sci. **124**, 1578–1588 (2012). https://doi.org/10.1002/app.35202

Poutrel, Q.-A., Wang, Z., Wang, D., Soutis, C., Gresil, M.: Effect of pre and post-dispersion on electro-thermo-mechanical properties of a graphene enhanced epoxy. Appl. Compos. Mater. **24**, 313–336 (2017). https://doi.org/10.1007/s10443-016-9541-0

Prolongo, S.G., Jimenez-Suarez, A., Moriche, R., Ureña, A.: In situ processing of epoxy composites reinforced with graphene nanoplatelets. Compos. Sci. Technol. **86**, 185–191 (2013). https://doi.org/10.1016/j.compscitech.2013.06.020

Qamar, S., Yasin, S., Ramzan, N., Iqbal, T., Akhtar, M.N.: Preparation of stable dispersion of graphene using copolymers: dispersity and aromaticity analysis. Soft Mater. **17**, 190–202 (2019). https://doi.org/10.1080/1539445X.2019.1583673

Shadlou, S., Ahmadi-Moghadam, B., Taheri, F.: The effect of strain-rate on the tensile and compressive behavior of graphene reinforced epoxy/nanocomposites. Mater. Des. **59**, 439–447 (2014). https://doi.org/10.1016/j.matdes.2014.03.020

Tan, H., Jiang, L.Y., Huang, Y., Liu, B., Hwang, K.C.: The effect of van der Waals-based interface cohesive law on carbon nanotube-reinforced composite materials. Compos. Sci. Technol. **67**, 2941–2946 (2007). https://doi.org/10.1016/j.compscitech.2007.05.016

Tang, L.-C., Wang, X., Gong, L.-X., Peng, K., Zhao, L., Chen, Q., Wu, L.-B., Jiang, J.-X., Lai, G.-Q.: Creep and recovery of polystyrene composites filled with graphene additives. Compos. Sci. Technol. **91**, 63–70 (2014). https://doi.org/10.1016/j.compscitech.2013.11.028

Wan, Y.-J., Tang, L.-C., Yan, D., Zhao, L., Li, Y.-B., Wu, L.-B., Jiang, J.-X., Lai, G.-Q.: Improved dispersion and interface in the graphene/epoxy composites via a facile surfactant-assisted process. Compos. Sci. Technol. **82**, 60–68 (2013). https://doi.org/10.1016/j.compscitech.2013.04.009

Wang, X., Jin, J., Song, M.: An investigation of the mechanism of graphene toughening epoxy. Carbon **65**, 324–333 (2013). https://doi.org/10.1016/j.carbon.2013.08.032

Wang, F., Drzal, L.T., Qin, Y., Huang, Z.: Mechanical properties and thermal conductivity of graphene nanoplatelet/epoxy composites. J. Mater. Sci. **50**, 1082–1093 (2015a). https://doi.org/10.1007/s10853-014-8665-6

Wang, X., Gong, L.-X., Tang, L.-C., Peng, K., Pei, Y.-B., Zhao, L., Wu, L.-B., Jiang, J.-X.: Temperature dependence of creep and recovery behaviors of polymer composites filled with chemically reduced graphene oxide. Composites, Part A, Appl. Sci. Manuf. **69**, 288–298 (2015b). https://doi.org/10.1016/j.compositesa.2014.11.031

Wu, Y., Wang, B., Ma, Y., Huang, Y., Li, N., Zhang, F., Chen, Y.: Efficient and large-scale synthesis of few-layered graphene using an arc-discharge method and conductivity studies of the resulting films. Nano Res. **3**, 661–669 (2010). https://doi.org/10.1007/s12274-010-0027-3

Yang, J., Zhang, Z., Friedrich, K., Schlarb, A.K.: Creep resistant polymer nanocomposites reinforced with multiwalled carbon nanotubes. Macromol. Rapid Commun. **28**, 955–961 (2007). https://doi.org/10.1002/marc.200600866

Zandiatashbar, A., Picu, C.R., Koratkar, N.: Control of epoxy creep using graphene. Small **8**, 1676–1682 (2012). https://doi.org/10.1002/smll.201102686

Zhang, W., Joshi, A., Wang, Z., Kane, R.S., Koratkar, N.: Creep mitigation in composites using carbon nanotube additives. Nanotechnology **18**, 185703 (2007). https://doi.org/10.1088/0957-4484/18/18/185703

Zhang, G., Wang, F., Dai, J., Huang, Z.: Effect of functionalization of graphene nanoplatelets on the mechanical and thermal properties of silicone rubber composites. Materials **9**, 92 (2016). https://doi.org/10.3390/ma9020092

Publisher's Note Springer Nature remains neutral with regard to jurisdictional claims in published maps and institutional affiliations.

Authors and Affiliations

Ozgen U. Colak[1] · Besim Birkan[1] · Okan Bakbak[1] · Alperen Acar[1] · Deniz Uzunsoy[2]

✉ O.U. Colak
ozgen@yildiz.edu.tr

B. Birkan
bbirkan@yildiz.edu.tr

O. Bakbak
obakbak@yildiz.edu.tr

A. Acar
alpacar@yildiz.edu.tr

D. Uzunsoy
deniz.uzunsoy@btu.edu.tr

1 Department of Mechanical Engineering, Yıldız Technical University, Istanbul, Turkey

2 Department of Metallurgy and Materials Engineering, Bursa Technical University, Bursa, Turkey